**THE EUROPEAN**
**PHYSICAL JOURNAL C**

# Leading neutron spectra

A.B. Kaidalov[1,2], V.A. Khoze[2,3,a], A.D. Martin[2], M.G. Ryskin[2,3]

[1] Institute of Theoretical and Experimental Physics, Moscow, 117259, Russia
[2] Department of Physics and Institute for Particle Physics Phenomenology, University of Durham, DH1 3LE, UK
[3] Petersburg Nuclear Physics Institute, Gatchina, St. Petersburg, 188300, Russia

**Abstract.** It is shown that the observation of the spectra of leading neutrons from proton beams can be a good probe of absorptive and migration effects. We quantify how these effects modify the reggeized pion-exchange description of the measurements of leading neutrons at HERA. We are able to obtain a satisfactory description of all the features of these data. We also briefly discuss the corresponding data for leading baryons produced in hadron–hadron collisions.

## 1 Introduction

Leading neutrons, which are produced from proton beams, are of special interest since the production process is dominated by $\pi$ exchange; see Sect. 2. Such leading neutron spectra have been measured recently in photon–proton collisions at HERA [1–5]. These data supplement measurements of leading baryon spectra made in hadron–hadron collisions many years ago [6–10]. By observing leading neutrons we have essentially a tagged $\pi$ beam. For example at HERA this $\pi$ beam may participate in deep inelastic scattering (DIS) or photoproduction. In this way both the structure function of the pion $F_2^\pi$ [2, 4] and the form of the underlying reggeized $\pi$ trajectory [3] can be studied.

There is another aspect of such processes which merits particular study. Soft rescattering effectively leads to the absorption of leading neutrons with Feynman variable $x$ (which we denote $x_L$) close to 1; the role of this correction was originally studied in [11, 12]. At that time, these were essentially theoretical studies, which provided predictions for future measurements.

Now detailed leading neutron data have become available from the experiments at HERA. These experiments measure the $\gamma^* p \to Xn$ cross sections for producing leading neutrons with different $x_L$ and $p_T$ values, as functions of both the virtuality, $Q^2$, of the photon, and the c.m. energy, $W$, of the incoming $\gamma p$ system. The HERA data offer the opportunity of seeing how absorption changes as a function of all these kinematic observables. We also show the importance of migration, or change of the kinematic variables, of the leading neutron due to rescattering effects. The ways to estimate the effects of absorption and of migration are discussed in Sects. 3 and 4 respectively. The description of the HERA data, $\gamma p \to Xn$, is presented in Sect. 5. For

completeness, in Sect. 6, we discuss the behavior of leading baryons produced in hadron–hadron collisions, in particular in the processes $pp \to Xn$ and $pn \to Xp$.

In exclusive reactions, the rescattering could produce new secondaries which has the effect of suppressing the rate. That is, an exclusive cross section is suppressed by absorptive effects. On the other hand, for an inclusive process the rescattering will just change the energy and transverse momentum of the leading baryon and will depopulate the region of large $x_L$ and small $p_T$. From the viewpoint of an experimental trigger, for $x_L \to 1$ this appears as absorption, but it is better to consider it as a migration into an enlarged phase space. In particular, such a migration can affect the form of the effective (that is measured) $\pi$ trajectory, leading to a larger mean $p_T$ at lower $x_L$. Of course, this may also modify the measurement of the pion structure function, $F_2^\pi$, which is extracted from the HERA data.

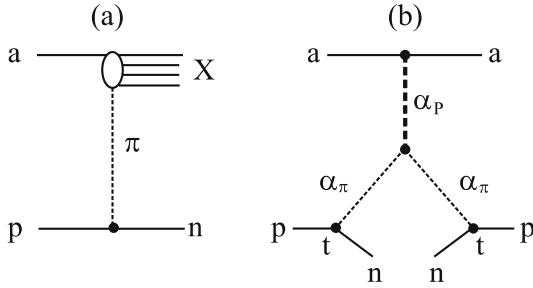## 2 Leading neutrons from $\pi$ exchange

To begin with, let us recall the triple-Regge formula which describes the inclusive processes $ap \to Xn$ with $a = \gamma$ or $p$. For $x_L$ close to unity the inclusive leading neutrons spectra is given by the triple-Regge diagrams shown in Fig. 1. Thus we have

$$f \equiv E \frac{\mathrm{d}^3\sigma}{\mathrm{d}^3 p} = \left(\frac{s}{s_0}\right)^{\alpha_P(0)-1} \frac{g_\pi^2(t) g_P(0) r_{P\pi\pi}(t)}{\sin^2(\pi\alpha_\pi(t))}$$
$$\times (1 - x_L)^{\alpha_P(0) - 2\alpha_\pi(t)}, \qquad (1)$$

where $t = (p_p - p_n)^2$; and $g_P(0)$ is the coupling of the pomeron to the photon, via a $q\bar{q}$ pair, or the proton, depending on whether $a = \gamma$ or $p$. The above form, with only the dominant pion-exchange contribution, has been

**Fig. 1. a** The pion-exchange amplitude and **b** the corresponding dominant triple-Regge contribution to the cross section of the inclusive production of leading neutrons, $ap \to Xn$. The coupling of the pomeron–$\pi$–$\pi$ Regge trajectories is denoted by $r_{P\pi\pi}(t)$ in (1)



**Fig. 2.** Diagrams **a** and **b** show the reggeized $\pi$-exchange contributions to the leading $ap \to XN$ and $ap \to X(N\pi)$ spectra respectively, with $N = p, n$

used by many authors, see, for example [2, 13, 14]. Moreover, both the old hadron–hadron interaction data and the recent HERA results on the spectra of neutrons [3] clearly indicate the reggeization of pion exchange. In fact, detailed studies of hadronic interactions in the reggeized pion-exchange model [13, 14] have shown that the formula can be used in a broad range of $x_L$, with $x_L \gtrsim 0.4$–$0.5$.

The contribution of reggeized pion exchange to the inclusive production of baryons, $ap \to XN$ with $N = p, n, ...$, is of the form

$$\frac{\mathrm{d}^2\sigma(ap \to XN)}{\mathrm{d}x_L \, \mathrm{d}t} = \frac{G^2_{\pi^+pn}(-t)}{16\pi^2 \left(t - m_\pi^2\right)^2} F^2(t) \sigma_{a\pi}^{\mathrm{tot}}(M^2)$$
$$\times (1 - x_L)^{1 - 2\alpha_\pi(t)} , \qquad (2)$$

where $\alpha_\pi(t) = \alpha'_\pi(t - m_\pi^2)$ is the pion trajectory with slope $\alpha'_\pi \simeq 1 \, \mathrm{GeV}^{-2}$, and $G^2_{\pi^0pp}/4\pi = G^2_{\pi^+pn}/8\pi = 13.75$ [15]. The invariant mass $M$ of the produced system $X$ is given by $M^2 \simeq s(1 - x_L)$. The signature factor and the difference between $\sin(\pi\alpha_\pi(t))$ and $(t - m_\pi^2)$ factors in the denominators of (1) and (2) are absorbed in the effective vertex form factor $F(t)$. This form factor is usually taken to be of the form

$$F(t) = \exp(bt/2) , \qquad (3)$$

where, from data at relatively low energies, we expect $b \sim 4 \, \mathrm{GeV}^{-2}$; see, for example, [14]. However more recent analyses find $b \sim 0$ [2, 16].

For the pion-exchange contributions to the spectra of both protons and neutrons, it is possible to take account, not only of the diagram of Fig. 2a, but also of the diagram of Fig. 2b. Besides this we can include the contributions of $\rho, a_2, ...$ exchanges, and also of resonance decays, such as the $\Delta$-resonance contribution in the $\pi N$ amplitude, to the leading $p$ and $n$ spectra. The calculations of the spectra of neutrons of [13, 14, 16] show that the diagram of Fig. 2a dominates and that the contribution of the diagram of Fig. 2b is about 20% at most. On the contrary, the leading proton spectrum is dominated by the triple-pomeron diagram; the diagram of Fig. 2a gives only about 30% of the inclusive cross section for $x_p \simeq 0.8$ in the ISR energy range.
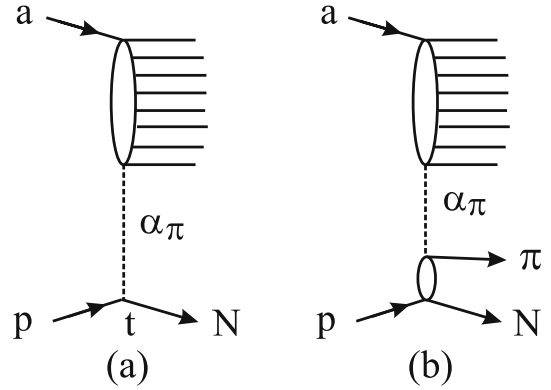
One interesting application of the leading neutron spectra at HERA is the possibility of using (2) to extract information on the $\gamma\pi$ total cross section, $\sigma_{\gamma\pi}^{\mathrm{tot}}$, for both real and virtual photons. This, in turn, allows for a measurement of the pion structure function $F_2^\pi(x_{\mathrm{Bj}}, Q^2)$ at very high energy or small Bjorken variable $x_{\mathrm{Bj}}$. The direct application of (2) to the HERA photoproduction data [2] leads to the result $\sigma_{\gamma\pi}^{\mathrm{tot}}/\sigma_{\gamma p}^{\mathrm{tot}} = 0.32 \pm 0.03$, which is about a factor 2 lower than the expected[1] ratio of $2/3$. However, so far, we have neglected the absorptive corrections, or so-called rescattering effects, to (2). These are very important at high energies. They reduce the predicted cross section, and they modify both the energy and the $Q^2$ dependence of the inclusive spectra of leading neutrons as well. We discuss the form of the correction in the next section and present the leading neutron spectra at HERA in Sect. 5.

## 3 Unitarity effects and gap survival

The Born-type Regge pole exchange diagram of Fig. 1 represents only the first approximation to the description of the leading neutron spectra at high energies. Multi-pomeron exchanges introduce modifications of the amplitudes and lead to the restoration of unitarity [18, 19].

We use the space-time diagram of Fig. 3 to distinguish between two types of rescattering. First we have the eikonal scattering of the leading hadrons (either incoming or outgoing) indicated by exchange (a). The other possibility is the rescattering of the leading hadron on one of the intermediate partons in the central rapidity region, indicated by exchange (b).

In terms of Feynman diagrams, an additional pomeron exchange leads to a negative contribution; that is, absorptive corrections diminish the size of the predicted cross

---

[1] Note that experimental estimates of $\sigma_{\pi p}^{\mathrm{tot}}$ at high energies, based on the absorptive corrections to the amplitude for $\gamma + p \to \pi^+\pi^- + p$ and its interference with the $\gamma + p \to \rho^0 + p$ amplitude, are about $\frac{2}{3}\sigma_{pp}^{\mathrm{tot}}$ at the same energy [17]. Thus we expect the additive quark model estimates to be reliable.
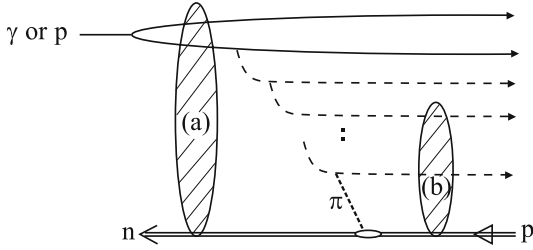
**Fig. 3.** The space-time diagram for the amplitude describing leading neutrons produced by the inclusive processes $\gamma p \to Xn$ or $pp \to Xn$. The two types of multi-pomeron absorptive corrections are indicated symbolically by the *shaded areas* (a) and (b). The corresponding corrections to the cross section are shown in Figs. 4 and 5 respectively

section. From the physical point of view, the inelastic interaction, shown by either exchange (a) or exchange (b) in Fig. 3, produces new secondary particles which populate the rapidity gaps and carry away energy from the leading neutron. In other words, a leading neutron, with a large energy fraction $x_L$, can only be observed in the small fraction of events which have no secondary inelastic interactions. The rescattering corrections therefore reduce the probability that the leading neutrons will be found in the large $x_L$ bins.

Technically the absorptive corrections are calculated in the following way. The most familiar ones are the eikonal-type corrections which are shown symbolically in Fig. 4, where only elastic rescatterings are taken into account. The corrections are well known:

$$d\sigma = \int \exp(-\Omega(s,\rho_T)) \, d\sigma_0(s,\rho_T...) \,, \qquad (4)$$

where $\rho_T$ is the impact parameter, and $d\sigma_0$ is the contribution to the cross section for leading neutron production from the lowest order diagram of Fig. 1b. The opacity $\Omega$ is the impact representation of the single-pomeron contribution to elastic scattering, which can be determined from studies of the total and elastic processes; for a recent review, see, for example, [20]. The formalism can easily be extended to take into account diffractive excitations of the initial and final hadrons. It leads to a multi-channel version of (4); see, for example, [18, 19, 21]. Diagrams of this eikonal type have been considered in previous estimates of absorptive corrections to the spectra of leading baryons [11, 12].

Note that since $\Omega(s,\rho_T)$ increases with energy, the suppression of the Born cross section $d\sigma_0$ also increases with energy. The damping factor, $\exp(-\Omega(s,\rho_T))$, is strongest for small values of the impact parameter $\rho_T$. Thus the absorptive suppression is greater for the $\rho, a_2$ reggeons than for $\pi$ exchange, which, due to the $1/(t-m_\pi^2)$ behavior at small $t$, has a broader distribution in $\rho_T$.

The unitarity corrections have an interesting effect on the $t$ dependence of the cross section driven by pion exchange, (2). As the pion pole is approached, that is, as $t \to m_\pi^2$, the corresponding impact parameter becomes very large, $\rho_T \to \infty$, and the gap survival damping factor behaves thus:

$$S^2(\rho_T) \equiv \exp(-\Omega) \to 1 \,. \qquad (5)$$

Thus we anticipate a more complicated $t$ dependence than that given by (2) and (3). First, at very small $t$, $|t| \lesssim 4m_\pi^2$, the survival factor $S^2$ rapidly decreases from $S^2 = 1$ at $t = m_\pi^2$, finally reaching a value $\sim \exp(-\Omega(\rho_t = 0))$ at large $|t|$. However, before that, the additional $t$ dependence coming from the pion vertex and trajectory reveals itself, namely $f_V(t) = \exp(bt/2)$ with $b \sim 1\,\mathrm{GeV}^2$. So, in (2), we have

$$F(t) = f_V(t)S(t) \,. \qquad (6)$$

Thus fitting the data using the single exponential form (3) may confuse the situation. Note that in the discussion below we will use the average value of $S^2$,

$$\hat{S}^2 = \langle \exp(-\Omega(\rho_T)) \rangle \,. \qquad (7)$$

Another class of multi-pomeron diagrams corresponds to the modification of the upper reggeon in the triple-pomeron diagram (Fig. 6a), or of the lower reggeons (Fig. 6b), or of both (Fig. 6c). The diagrams of Fig. 6a modify only the $M^2$ dependence of the cross sections, and for the $\pi$-exchange model can be absorbed in the behavior of $\sigma_{\pi a}^{\mathrm{tot}}(M^2)$. The diagrams of Fig. 6b modify the $x_L$ dependence, and for the $\pi$ case can be dealt with by modifying the $\pi$ trajectory (essentially the slope $\alpha_\pi'$) and the form factor. It is important that, to a good approximation, they do not depend on the energy[2] $\sqrt{s}$.

The multi-pomeron diagrams of Fig. 5 are only expected to become relevant at sufficiently high energies. That is when the energy is large enough for the mass $M$ of the pro-

---

[2] The unfactorizable diagram Fig. 6c can, in principle, have some weak $s$ dependence.
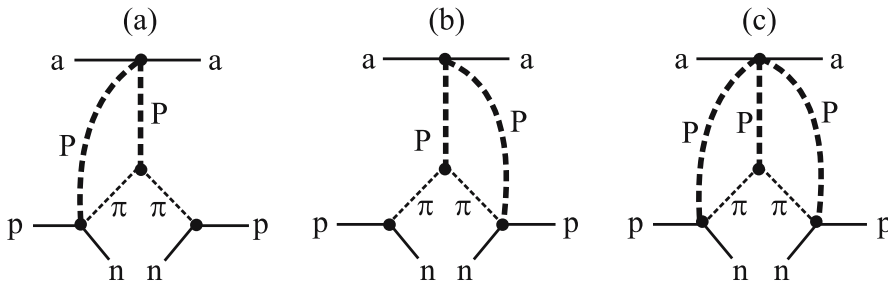


**Fig. 4.** Symbolic diagrams of the eikonal absorptive corrections to the cross section for the inclusive process $ap \to Xn$. The *extra lines* denoted by $P$, which surround the triple-Regge interaction, represent multi-pomeron exchanges between the leading hadrons
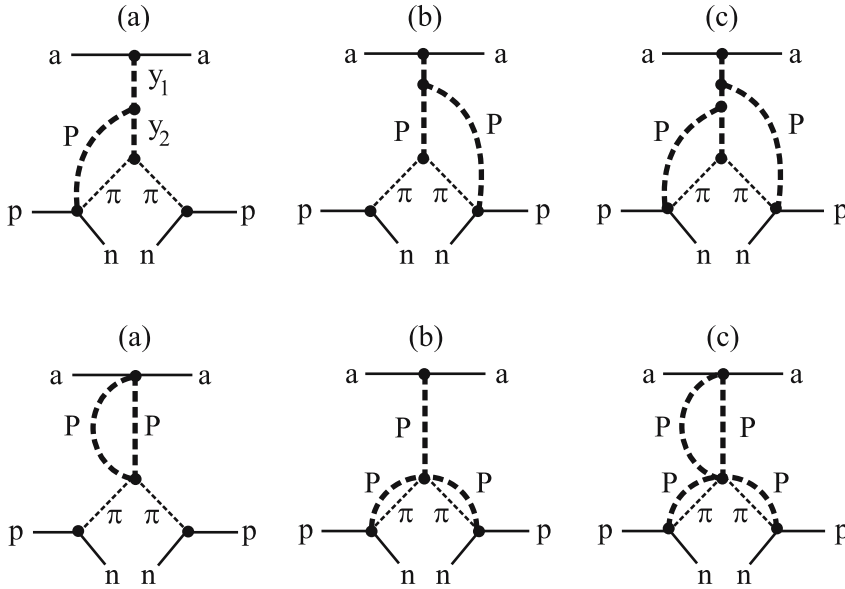
**Fig. 5.** Symbolic diagrams for the "enhanced" absorptive corrections to the cross section for the inclusive process $ap \to Xn$, which become important at very high energies. The mass $M$ of the produced system $X$ is assumed to be sufficiently large for both the rapidity intervals $y_1$ and $y_2$ to accommodate Pomeron exchange. The *extra lines* denoted by $P$, which are coupled directly to the ingoing $p$ or outgoing $n$, represent multi-pomeron exchanges



**Fig. 6.** Multi-pomeron corrections to the reggeons in the triple-regge diagrams. They have no, or at most a weak, dependence on energy. The *curved lines* denoted by $P$ represent multi-pomeron exchanges

duced system $X$ to itself be large enough for both the rapidity intervals $y_1$ and $y_2 = y_M - y_1$ to be sufficiently large to accommodate pomeron exchange[3]; that is $y_i \geq y_0$ with $y_0 \simeq 2$–3. Recall that $y_M = \ln(M^2/M_0^2)$ with $M_0^2 = 1 GeV^2$; so for a typical value of $M^2 \sim 3000 \, \mathrm{GeV}^2$ we have $y_M = y_1 + y_2 \sim 8$. Note that rapidity intervals $y_i < y_0$ are included in the contributions of the diagrams of Fig. 4 and Fig. 6b.

Let us study in more detail the diagram shown in Fig. 5a, which describes the process $ap \to Xn$. This diagram is one of the $s$-channel discontinuities of the triple-pomeron diagram for the elastic $ap$ scattering amplitude[4]; see Fig. 7. Indeed the diagram is related to the triple-pomeron diagram for the elastic amplitude by the AGK cutting rules [24]. The corresponding coefficient is 4. So it is straightforward to obtain the correction to the $ap \to Xn$ cross section from diagram of Fig. 5a, provided we know the cross section of Fig. 7 in the triple-pomeron region, $x_L \to 1$. By fitting this cross section to the triple-pomeron formula we can extract the strength of the vertex $r_{PPP}$ [25]. If we take the value of the effective vertex $r_{PPP}$ determined in the analysis of the old hadron data, then we find the correction due to the enhanced absorptive diagrams to be about 15%.

So there is a relatively small contribution coming from the enhanced graphs of Fig. 5; that is, from the rescattering of intermediate partons, as indicated by the shaded region (b) of Fig. 3. This is consistent with the fact that within the HERA range ($W = 40$–270 GeV) no energy dependence is observed in the leading neutron yields; see, for example, Fig. 6 of [5][5], and Tables 14, 18 and Figs. 11, 12 of [2]
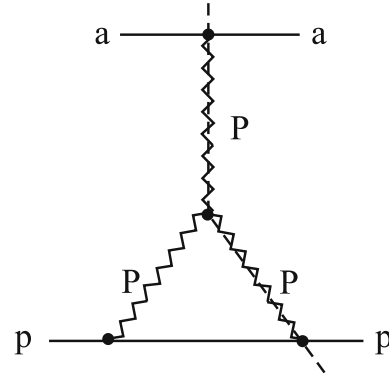


**Fig. 7.** A cut leading to an $s$-channel discontinuity of the triple-pomeron diagram for the elastic $ap$ scattering amplitude

which show, for fixed $Q^2$, the same probability[6] to observe a leading neutron for values of $x_{Bj}$ which decrease by more than an order of magnitude corresponding to an increase of the photon laboratory energy by more than a factor of 10. This flat experimental behavior of the probability indicates that actually the absorptive corrections caused by the rescattering of intermediate partons are much smaller than might be expected from leading order perturbative QCD calculations, similar to those presented in [26] (see also the discussion in [27,28]).

## 4 The inclusion of migration

In order to compute the spectra of leading neutrons, we must consider the effects of migration, as well as of absorption. We assume that each rescattering spreads out the $p_T, x_L$ spectra of the leading baryon according to

---

[3]　Diagrams of this type were mentioned in our paper on dijet production at the Tevatron [18], but for this hard diffractive process they were small even at Tevatron energies.

[4]　The summation of more complicated enhanced diagrams was discussed in [22], and more recently in [23].

[5]　See also Figs. 2 and 4 of [5] for leading proton data, where the effect of enhanced diagrams should be the same.

[6]　That is the same probability, $\hat{S}^2$, to observe the rapidity gap associated with pion exchange.

distribution[7]

$$\frac{\mathrm{d}N}{\mathrm{d}p_\mathrm{T}^2\,\mathrm{d}x_\mathrm{L}} = (1-a)x_\mathrm{L}^{-a}b_\mathrm{m}\exp(-p_\mathrm{T}^2 b_\mathrm{m})\,, \qquad (8)$$

where we take the slope $b_\mathrm{m} = 6\,\mathrm{GeV}^{-2}$, and the intercept $a \sim 0 - \frac{1}{2}$ corresponding to secondary reggeon exchange in the Kancheli–Mueller approach. Thus, after two rescatterings

$$\begin{aligned}\frac{\mathrm{d}N^{(2)}}{\mathrm{d}p_\mathrm{T}^2\,\mathrm{d}x_\mathrm{L}} &= b_\mathrm{m}^2\int\frac{\mathrm{d}^2 q_\mathrm{T}}{\pi}\exp(-q_\mathrm{T}^2 b_\mathrm{m})\exp(-(\mathbf{p}_\mathrm{T}-\mathbf{q}_\mathrm{T})^2 b_\mathrm{m}) \\ &\quad \times \int_0^1 \frac{\mathrm{d}x_1\,\mathrm{d}x_2}{(x_1 x_2)^a}(1-a)^2\delta(x_\mathrm{L}-x_1 x_2) \\ &= \frac{b_\mathrm{m}(1-a)^2\ln(1/x_\mathrm{L})}{2(x_\mathrm{L})^a}\exp(-p_\mathrm{T}^2 b_\mathrm{m}/2)\,.\end{aligned} \qquad (9)$$

Correspondingly, after $k$ rescatterings the distribution becomes

$$\frac{\mathrm{d}N^{(k)}}{\mathrm{d}p_\mathrm{T}^2\,\mathrm{d}x_\mathrm{L}} = \frac{b_\mathrm{m}(1-a)^k\ln^{k-1}(1/x_\mathrm{L})}{k(k-1)!(x_\mathrm{L})^a}\exp(-p_\mathrm{T}^2 b_\mathrm{m}/k)\,. \qquad (10)$$

The probability of rescattering, or, equivalently, the mean number $\nu$ of rescatterings, at fixed impact parameter $\rho_\mathrm{T}$ is given by the opacity $\nu \equiv \Omega$:

$$\Omega(\rho_\mathrm{T}) = \frac{\sigma(s)}{4\pi B_\mathrm{r}}\exp(-\rho_\mathrm{T}^2/4B_\mathrm{r})\,. \qquad (11)$$

Here we focus attention on migration effects in $\gamma p \to Xn$, so $\rho_\mathrm{T} \equiv \rho_{\gamma N}$. The cross section $\sigma$ is, however, not the $\gamma N$ total cross section, since the process proceeds in two stages. First the photon fluctuates into a $q\bar{q}$ pair, which may be considered as a sum of vector mesons, and then the vector mesons rescatter on a nucleon. We therefore assume $\sigma$ is the $\pi p$ total cross section having in mind the additive quark model and/or $\rho$ meson dominance. $B_\mathrm{r}$ is the slope of the rescattering amplitude (which we take to be $B_\mathrm{r} = 5\,\mathrm{GeV}^{-2}$).

Note that the impact parameter $\rho_\mathrm{T}$ in (11), which controls the absorption and migration effects, is not equal to the parameter $\rho_{\pi N}$ which describes the space structure of "pure" one-pion exchange in leading neutron production. The subscript $\pi$ denotes the "transverse" position of the $\pi$–$\pi$–pomeron vertex in Fig. 1b. That is, $\rho_{\pi N}$ is the Fourier conjugate of the neutron transverse momentum in the bare (Born) amplitude leading to the cross section in (2). However, due to the rather large values of

$\rho_{\pi N}$, we may expect that the absorptive and migration effects will not be too strong – since the transverse distance between the leading baryon and the incoming photon (or $q\bar{q}$-pair),

$$\rho_\mathrm{T} \equiv \rho_{\gamma N} = |\boldsymbol{\rho}_{\pi N}+\boldsymbol{\rho}_{\gamma\pi}|\,, \qquad (12)$$

is, in turn, relatively large, and the mean number of rescatterings $\nu(\rho_\mathrm{T}) = \Omega(\rho_\mathrm{T})$ at the periphery of the interaction (described by the amplitude $\Omega$) is rather small. Here $\rho_{\gamma\pi}$ is the impact parameter for the amplitude describing the interaction of the incoming photon with the "effective" pion (exchanged in the $t$-channel); recall that the subscript $\pi$ denotes the position of the $\pi$–$\pi$–pomeron vertex in Fig. 4.

To account for the fact that $\rho_\mathrm{T}$ and $\rho_{\pi N}$ are not the same, for each value of $\rho_{\pi N}$, we calculate the probability

$$\begin{aligned}w(\rho_\mathrm{T},\rho_{\pi N}) &= N(\rho_{\pi N}) \\ &\quad \times \int \mathrm{d}^2\rho_{\gamma\pi}\Omega_\pi(\rho_{\gamma\pi})\delta(\rho_\mathrm{T}-|\boldsymbol{\rho}_{\gamma\pi}+\boldsymbol{\rho}_{\pi N}|)\,,\end{aligned} \qquad (13)$$

where $\Omega_\pi(\rho_{\gamma\pi})$ is the amplitude in impact parameter space for the photon–pion interaction. It is of the form (11) with the same slope $B_\mathrm{eff} = B_\mathrm{r} = 5\,\mathrm{GeV}^{-2}$. Since the expression (2) already includes the probability of the "effective" pion–$\gamma$ interaction, the probabilities $w(\rho_\mathrm{T},\rho_{\pi N})$ are normalized to one; that is the normalization $N(\rho_{\pi N})$ is fixed by the condition[8]

$$\int \mathrm{d}\rho_\mathrm{T} w(\rho_\mathrm{T},\rho_{\pi N}) = 1 \qquad (14)$$

for every value of $\rho_{\pi N}$.

Thus, to calculate the inclusive cross section for leading neutron production we have to integrate over the impact parameter $\rho_\mathrm{T}$

$$\begin{aligned}\frac{\mathrm{d}\sigma}{\mathrm{d}x_\mathrm{L}\,\mathrm{d}p_\mathrm{T}^2} &= \int \mathrm{d}^2\rho_\mathrm{T}\frac{\exp(\mathrm{i}\mathbf{p}_\mathrm{T}\cdot\boldsymbol{\rho}_{\pi N})}{2\pi}\mathrm{d}^2\rho_{\pi N}w(\rho_\mathrm{T},\rho_{\pi N}) \\ &\quad \times \mathcal{F}(\rho_\mathrm{T},\rho_{\pi N},x_\mathrm{L})\,,\end{aligned} \qquad (15)$$

---

[7] Strictly speaking, besides the migration in $p_\mathrm{T},x_\mathrm{L}$ space, there may be charge exchange (that is, neutron to proton transitions). We neglect this effect since the goal of the present section is not a precise quantitative description, but rather a qualitative evaluation of the role and possible size of the "migration" phenomenon. For the same reason we use a simplified form, (8), of the leading baryon distribution.

[8] Strictly speaking we should work with amplitudes and not with cross sections. Moreover the impact parameter $\rho_\mathrm{T}$ in the amplitude $A$ may not be equal to the parameter $\rho_\mathrm{T}^*$ in the conjugated amplitude $A^*$. We find $\rho_\mathrm{T} = \rho_\mathrm{T}^*$ only after integration over the neutron transverse momentun $p_\mathrm{T}$. However to simplify the computations, here we use the semiclassical approximation, which assumes $\rho_\mathrm{T} = \rho_\mathrm{T}^*$, using the Fourier transform just for the cross section. This approach, which is usually used in Monte Carlo simulations, may be justified by the fact that the effect of migration becomes important only at relatively large $p_\mathrm{T}$, see Fig. 8. So after we integrate up to $p_\mathrm{T} = 0.5$–$1\,\mathrm{GeV}$ we find that the equality $\rho_\mathrm{T} = \rho_\mathrm{T}^*$ holds to rather good accuracy. Nevertheless, the fact that we need to correct the normalization in (13) and (14) is just the result of this semiclassical approximation.

where

$$\mathcal{F}(\rho_{\mathrm{T}}, \rho_{\pi N}, x_{\mathrm{L}}) = \nu(\rho_{\mathrm{T}}) \, \mathrm{e}^{-\nu(\rho_{\mathrm{T}})} \left[ \mathcal{F}^{(0)}(\rho_{\pi N}, x_{\mathrm{L}}) \right.$$
$$\left. + \int_{x_{\mathrm{L}}}^{1} \mathrm{d}x'_{\mathrm{L}} \mathcal{F}^{(0)}(\rho_{\pi N}, x'_{\mathrm{L}}) \mathcal{F}^{(\mathrm{r})}(\rho_{\pi N}, x_{\mathrm{L}}/x'_{\mathrm{L}}) \right] . \quad (16)$$

The factor $\nu(\rho_{\mathrm{T}}) \exp(-\nu(\rho_{\mathrm{T}}))$ accounts for the probability of the first interaction and the absorption at a given impact parameter $\rho_{\mathrm{T}}$, where $\nu(\rho_{\mathrm{T}}) = \Omega(\rho_{\mathrm{T}})$ is the mean number of interactions. The first term in the square brackets, $\mathcal{F}^{(0)}$, is the original cross section (2) in the $\rho_{\pi N}$ representation; that is,

$$\mathcal{F}^{(0)}(\rho_{\pi N}, x_{\mathrm{L}}) = \int \frac{\mathrm{d}^2 p_{\mathrm{T}}}{2\pi} \exp(\mathrm{i} \mathbf{p}_{\mathrm{T}} \cdot \rho_{\pi N}) \frac{\mathrm{d}\sigma^{(0)}}{\mathrm{d}x_{\mathrm{L}} \, \mathrm{d}p_{\mathrm{T}}^2} .$$

The second term function $\mathcal{F}^{(\mathrm{r})}$ accounts for the migration. When we sum over $k = 1, 2, \dots$ rescatterings, the spectra in the $\rho_{\pi n}$ representation take the form

$$\frac{\mathrm{d}N}{\mathrm{d}p_{\mathrm{T}}^2 \, \mathrm{d}x_{\mathrm{L}}} = \sum_{k=1}^{\infty} \frac{\mathrm{d}N^{(k)}}{\mathrm{d}p_{\mathrm{T}}^2 \, \mathrm{d}x_{\mathrm{L}}}$$
$$= \int \frac{\mathrm{d}^2 \rho}{2\pi} \exp(\mathrm{i} \mathbf{p}_{\mathrm{T}} \cdot \boldsymbol{\rho})$$
$$\times \sum_{k=1}^{\infty} (\nu e^{-\rho^2/4b_{\mathrm{m}}})^k \frac{(1-a)^k \ln^{k-1}(1/x_{\mathrm{L}})}{(k-1)!(x_{\mathrm{L}})^a}$$
$$= \int \frac{\mathrm{d}^2 \rho}{2\pi} \exp(\mathrm{i} \mathbf{p}_{\mathrm{T}} \cdot \boldsymbol{\rho}) \nu(1-a) e^{-\rho^2/4b_{\mathrm{m}}}$$
$$\times \exp\left( \nu(1-a) e^{-\rho^2/4b_{\mathrm{m}}} \ln(1/x_{\mathrm{L}}) \right) /(x_{\mathrm{L}})^a . \quad (17)$$

Thus the function $\mathcal{F}^{(\mathrm{r})}$ in (16) is

$$\mathcal{F}^{(\mathrm{r})}(\rho, x_{\mathrm{L}}) = \nu(1-a) e^{-\rho^2/4b_{\mathrm{m}}}$$
$$\times \exp\left( \nu(1-a) e^{-\rho^2/4b_{\mathrm{m}}} \ln(1/x_{\mathrm{L}}) \right) /(x_{\mathrm{L}})^a . \quad (18)$$

The results shown below correspond to $a = 0$, but the spectra obtained for $a = \frac{1}{2}$ are very similar.

## 5 Predictions for leading neutrons at HERA

To predict the absorptive corrections to the pion-exchange formula (2), in which we set $b = 0$, we use (4), together with (11) in which we take $\sigma = 1.3 \times 31$ mb. The value $\sigma_{\mathrm{tot}}(\pi p) = 31$ mb agrees with the Donnachie–Landshoff parametrization [29] and with the cross section evaluated by ZEUS via the $\pi$–proton absorption in $\gamma p \to (\pi^+ \pi^-) \, p$ process [17]. The factor 1.3 takes account of the diffractive excitations of the initial and final hadrons [30].

The resulting predictions for the $x_{\mathrm{L}}$ spectra of leading neutrons produced at HERA are shown in Fig. 8. In the first plot the ZEUS acceptance cut, $\theta_n < 0.8$ mrad, has

been imposed. In the next three plots we show the effect of imposing different $p_{\mathrm{T}}$ cuts, rather than the $\theta_n$ cut, on the leading neutron. Each plot shows three curves. The dotted curve is the reggeized $\pi$-exchange prediction calculated from (2), whereas the continuous and dashed curves are computed from (15) and (16) with and without migration ($\mathcal{F}^{(\mathrm{r})}$) included. The data points correspond to the leading neutron spectra measured by ZEUS [2].

As anticipated, the migration practically does not affect the region of large $x_{\mathrm{L}} > 0.8$, where it is essentially enough to account for absorption only. However, at smaller $x_{\mathrm{L}}$ the role of migration becomes quite important. First of all, it compensates for the absorption (which occurs for $x_{\mathrm{L}}$ close to 1) and provides the conservation of baryon charge. Next, it changes the behavior of the $x_{\mathrm{L}}$ and $p_{\mathrm{T}}$ distributions of the leading neutrons and modifies the "effective" slope of the reggeized pion trajectory which was extracted from the data using the simplified formula (2).

From Fig. 8, we see that the predicted leading neutron spectrum is in satisfactory agreement with that measured by ZEUS. The absorptive corrections reduce the cross section given simply by reggeized pion exchange by a factor of about 0.4 so that the predictions are in agreement with the data at large $x_{\mathrm{L}}$. The reduction by 0.4 is in line with an earlier calculation [31] which gave a rapidity gap survival factor $\hat{S}^2$ of 0.34 for the resolved part of the photon wave function.

Moreover the data on the production of a leading neutron, together with either a pair of high $E_{\mathrm{T}}$ jets [32] or charm ($D^*$) [33], are consistent with a much larger value of $\hat{S}^2$, as is to be expected when we select $x_\gamma \to 1$ events which sample a point-like photon, which directly interacts with high $E_{\mathrm{T}}$ dijets. In particular, the probability to observe a leading neutron increases by up to a factor of 2.5 (that is, $\hat{S}^2$ increases up to about 0.9) when the momentum fraction carried by the dijet grows from 0 to 1; see Fig. 8c of [32]. In [34] the H1 dijet data were described, within NLO QCD [35], by pure pion exchange without the inclusion of the survival factor; that is, with $\hat{S}^2 = 1$. However the $t$ dependence was not studied. Moreover a larger $t$-slope parameter, $R = 0.93 \, \mathrm{GeV}^{-1}$, was used in [34] than the value $R = 0.5 \, \mathrm{GeV}^{-1}$ used in [35]. Thus the $b$ slope in [34] is 3.5 times larger. In this way the absorptive corrections were mimicked in [34]; see the discussion leading to (6).

The comparison with the ZEUS data in Fig. 8 shows evidence of migration for $0.4 \lesssim x_{\mathrm{L}} \lesssim 0.6$. The points at lower $x_{\mathrm{L}}$ indicate that there may be additional contributions[9] caused by the recombination of an initial valence quark with a sea quark in the neutron with $x_{\mathrm{L}} \sim 0.3$, as well as by baryon charge transfer to the central region[10], whose description is beyond the present analysis.

The leading neutron measurements at HERA also allow us to explore the $Q^2$ dependence of the problem. Unlike the naive vector dominance model (VDM), where the effect of

---

[9] Note that in our computation we have already used $b = 0$. Thus we have no possibility to enlarge the neutron yield for $x_{\mathrm{L}} \sim 0.5$ by diminishing the value that we take for the slope $b$.

[10] The ratio $p/\bar{p} > 1$ measured in the central region at RHIC and HERA indicates the presence of such an effect.
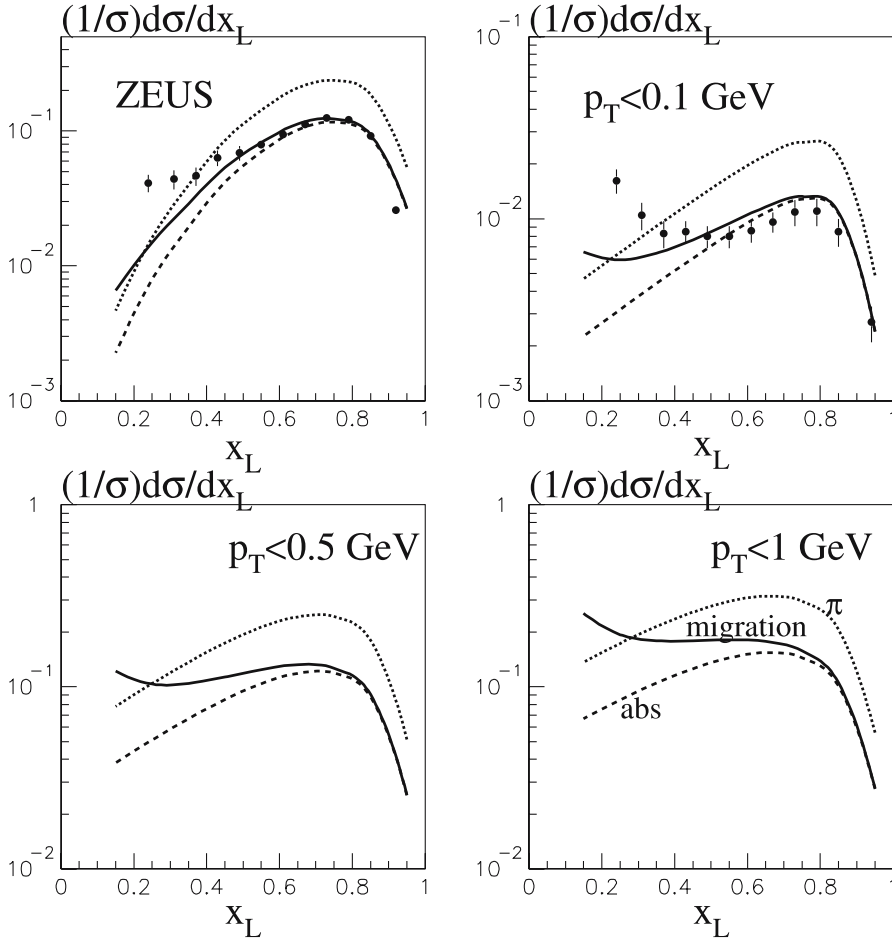
**Fig. 8.** The predictions for the $x_L$ spectra of leading neutrons corresponding to the ZEUS kinematics. The *dotted*, *dashed* and *continuous curves* are respectively the results assuming first only reggeized $\pi$ exchange, then including absorptive effects, and finally allowing for migration. The different plots show the effects of imposing different $p_T$ cuts on the leading neutron. The data points are the spectra obtained from the measurements of [2]. Note that the curves plotted here account only for the pion-exchange contribution, which is not the dominant source of leading neutrons for $x_L \lesssim 0.4$

absorption should disappear as $1/Q^2$, in QCD (or in the generalized VDM) these effects are expected to decrease as $1/\ln Q^2$. It was shown in [2] that the $Q^2$ behavior observed at HERA is consistent with predictions [11, 12] based on the QCD dipole approach.

## 6 Leading baryon spectra in hadron–hadron collisions

Some years before the HERA data became available, leading nucleon spectra had been observed in hadron–hadron collisions in a variety of experiments, albeit at lower energies. Generally, these and related data are well described by the triple-reggeon formalism. At first sight, it seems to be strange that no gap survival factor suppression, $\hat{S}^2$, was necessary – particularly in view of our discussion of the HERA data in the previous section. However, this factor is effectively included in the normalization of the triple-reggeon vertices [25] which were determined by fitting the data. The only problem is the $\pi$–$\pi$–pomeron vertex, which must be consistent with the known result for the on-shell pion as $t \to m_\pi^2$. The on-shell vertex is known from an independent analysis of $\pi p$ total and differential cross section data. Now, it is crucial to note that the $\pi$–$\pi$–pomeron vertex depends strongly on

the value of $t - m_\pi^2$, leading to an effective factor $F(t) = 1$ at $t = m_\pi^2$. In the physical region of negative $t$ this factor is expected to be $\hat{S}^2 \sim 0.4$ in the CERN ISR energy range [30, 36, 37]. Indeed, the indications for such absorptive corrections to $\pi$ exchange were observed in data for $pp \to X\Delta^{++}$ production [8, 36]. Spectra of leading baryons in the reggeized pion-exchange model have been described in [13, 16, 36–39]. In [13, 38, 39] a phenomenological form factor, which to some extent mimic absorptive effects, has been used.

The situation with inclusive nucleon-charge exchange in $pp$ (and $pd$) collisions, that is, in the spectra of neutrons in $pp$ collisions and protons in $pn$ collisions, is not clear. The largest set of the highest energy data was obtained at the CERN ISR, [6] and [7]. These ISR spectra of neutrons have a rather different form. It was emphasized in [38] that the data of [6] are very different[11] from predictions of the pion-exchange model and lead to a violation of the energy-momentum sum rule, while the data of [7] are in reasonable agreement with theoretical predictions [39]. As mentioned above, the models of [38, 39] are based on reggeized pion exchange, with the gap survival factor $\hat{S}^2$ represented by a form factor which, however,

---

[11] Note that in the CERN ISR paper [6] the cross section plotted in Fig. 7 is about 3 times smaller than that given in the tables and in Fig. 6.

gave only a rather small effect ($\sim 10\%$). The equivalent process $pn \to Xp$ was also measured [9] over a range of energies, which partly overlap with the ISR energy range and are consistent with the model of [38]. On the other hand there are data on the process $pn \to Xp$ at relatively low energies (11.6 GeV), which are lower than predictions of the pion-exchange model without the $\hat{S}^2$ factor.

Thus the final picture for hadron–hadron processes is not clear. Some experiments are in agreement with the theoretical expectations of appreciable absorptive corrections to $\pi$ exchange, while others appear to be described by simplified $\pi$ exchange.

# 7 Summary

We have described all the main features of the leading neutrons observed at HERA, both in photoproduction and as a function of $Q^2$. For photoproduction we may refer to Fig. 8. We see that reggeized pion exchange on its own is insufficient to describe the production of leading neutrons. However the inclusion of absorptive corrections are found to reduce the $\pi$-exchange prediction by a factor of 0.4 and to bring the theoretical expectation in line with the data. Thus, after accounting for the rapidity gap survival factor $\hat{S}^2$, such data can be used to measure the $\gamma\pi$ cross section and the pion structure function. Moreover the value of the gap survival factor $\hat{S}^2$ may be monitored by comparing the spectra of leading neutrons in dijet production at low $x_\gamma$ with those for $x_\gamma \to 1$, where the cross section is dominated by the direct, point-like photon. Next, the dependence of the survival factor $\hat{S}^2$ (which specifies the probability to observe a leading neutron) on the photon energy may be used to experimentally probe the contribution of the enhanced absorptive corrections of Fig. 5. The data appear to be flat in energy indicating only a small contribution from enhanced absorptive corrections. This is relevant to the proposed Higgs searches in exclusive diffractive production at the LHC. Thus we can argue that the additional suppression of exclusive Higgs cross section caused by the enhanced diagrams cannot be as large as mentioned in [26], see [28] for a detailed discussion.

We also found that the neutron spectrum shows some evidence of migration effects; see Fig. 8. Including migration slightly reduces the value extracted for the slope of the pion Regge trajectory; the reduction is about $0.05$–$0.1\,\mathrm{GeV}^{-2}$ depending on the interval of $x_L$ used to measure $\alpha'_\pi$.

Finally, in Sect. 6, we briefly reviewed the available experimental data for leading baryons produced in hadron–hadron interactions, which were obtained about 30 years ago. Here the experimental situation is confusing. Some experiments are in line with theoretical expectations, while others are not.

# References

1. ZEUS Collaboration, M. Derrick et al., Phys. Lett. B **384**, 388 (1996); J. Breitweg et al., Nucl. Phys. B **596**, 3 (2001); Eur. Phys. J. C **1**, 81 (1998); ibid. C **2**, 237 (1998)
2. ZEUS Collaboration, S. Chekanov et al., Nucl. Phys. B **637**, 3 (2002)
3. ZEUS Collaboration, S. Chekanov et al., Phys. Lett. B **610**, 199 (2005)
4. H1 Collaboration, C. Adloff et al., Eur. Phys. J. C **6**, 587 (1999)
5. H1 Collaboration, C. Adloff et al., Nucl. Phys. B **619**, 3 (2001)
6. J. Engler et al., Nucl. Phys. B **84**, 70 (1975)
7. W. Flauger, F. Monnig, Nucl. Phys. B **109**, 347 (1976)
8. S.J. Barish et al., Phys. Rev. D **12**, 1260 (1975)
9. B. Robinson et al., Phys. Rev. Lett. **34**, 1475 (1975)
10. Y. Eisenberg et al., Nucl. Phys. B **135**, 189 (1978)
11. N.N. Nikolaev, J. Speth, B.G. Zakharov, hep-ph/9708290
12. U.D. Alesio, H.J. Pirner, Eur. Phys. J. A **7**, 109 (2000)
13. K.G. Boreskov, A.B. Kaidalov, L.A. Ponomarev, Sov. J. Nucl. Phys. **19**, 565 (1974)
14. K.G. Boreskov, A.B. Kaidalov, V.I. Lisin, E.S. Nikolaevskii, L.A. Ponomarev, Sov. J. Nucl. Phys. **15**, 203 (1972); L.A. Ponomarev, Sov. J. Part. Nucl. **7**, 70 (1976)
15. V. Stoks, R. Timmermans, J.J. de Swart, Phys. Rev. C **47**, 512 (1993); R.A. Arndt, I.I. Strakovsky, R.L. Workman, M.M. Pavan, Phys. Rev. C **52**, 2120 (1995)
16. B.Z. Kopeliovich, B. Povh, I. Potashnikova, Z. Phys. C **73**, 125 (1996)
17. ZEUS Collaboration, J. Breitweg et al., Eur. Phys. J. C **2**, 247 (1998)
18. A.B. Kaidalov, V.A. Khoze, A.D. Martin, M.G. Ryskin, Eur. Phys. J. C **21**, 521 (2001)
19. A.B. Kaidalov, Phys. Rep. **50**, 157 (1979); S.N. Ganguli, D.P. Roy, Phys. Rep. **67**, 201 (1980)
20. E. Gotsman, E. Levin, U. Maor, E. Naftali, A. Prygarin, in: HERA and the LHC, CERN-2005-014, p. 221
21. K.A. Ter-Martirosyan, ITEP preprints **70**, 71 (1975); **7**, 11, 133-135, 158 (1976)
22. A. Schwimmer, Nucl. Phys. B **94**, 445 (1975)
23. K.G. Boreskov et al., Eur. Phys. J. C **44**, 523 (2005); Y.V. Kovchegov, E. Levin, Nucl. Phys. B **577**, 221 (2000); S. Bondarenko, E. Gotsman, E. Levin, U. Maor, Nucl. Phys. A **683**, 644 (2001)
24. V. Abramovsky, V.N. Gribov, O.V. Kancheli, Sov. J. Nucl. Phys. **18**, 308 (1974)
25. A.B. Kaidalov, V.A. Khoze, Y.F. Pirogov, N.L. Ter-Isaakyan, Phys. Lett. **45**, 493 (1973); R.D. Field, G.C. Fox, Nucl. Phys. B **80**, 367 (1974)
26. J. Bartels, S. Bondarenko, K. Kutak, L. Motyka, Phys. Rev. D **73**, 093 004 (2006) [arXiv:hep-ph/0601128]
27. A.D. Martin, M.G. Ryskin, In: HERA and the LHC, CERN-2005-014, p. 369

28. V.A. Khoze, A.D. Martin, M.G. Ryskin, JHEP **0605**, 036 (2006) [arXiv:hep-ph/ 060-2247]
29. A. Donnachie, P.V. Landshoff, Phys. Lett. B **296**, 227 (1992)
30. V.A. Khoze, A.D. Martin, M.G. Ryskin, Eur. Phys. J. C **18**, 167 (2000); A.B. Kaidalov, Phys. Rep. **50**, 157 (1979)
31. A.B. Kaidalov, V.A. Khoze, A.D. Martin, M.G. Ryskin, Phys. Lett. B **567**, 61 (2003)
32. ZEUS Collaboration, J. Breitweg et al., Nucl. Phys. B **596**, 3 (2001)
33. ZEUS Collaboration, S. Chekanov et al., Phys. Lett. B **590**, 143 (2004)
34. H1 Collaboration, A. Aktas et al., Eur. Phys. J. C **41**, 273 (2005)
35. M. Klasen, G. Kramer, Phys. Lett. B **508**, 259 (2001)
36. K.J.M. Moriarty, J.H. Tabor, A. Ungkichanukit, Phys. Rev. D **16**, 130 (1977)
37. B.G. Zakharov, V.N. Sergeev, Sov. J. Nucl. Phys. **28**, 689 (1978); A.G. Azcarate, Phys. Rev. D **17**, 3022 (1978); B.G. Zakharov, V.N. Sergeev, Sov. J. Nucl. Phys. **38**, 801 (1983)
38. K.G. Boreskov, A.A. Grigorian, A.B. Kaidalov, Sov. J. Nucl. Phys. **24**, 411 (1976)
39. K.G. Boreskov, A.A. Grigorian, A.B. Kaidalov, I.I. Levintov, Sov. J. Nucl. Phys. **27**, 813 (1978)